In vivo characterization of lamina cribrosa pore morphology in primary open-angle glaucoma

Stéphanie Zwillinger, M. Paques, B. Safran, C. Baudouin

▶ **To cite this version:**

Stéphanie Zwillinger, M. Paques, B. Safran, C. Baudouin. In vivo characterization of lamina cribrosa pore morphology in primary open-angle glaucoma. Journal Français d'Ophtalmologie, 2016, 39 (3), 10.1016/j.jfo.2015.11.006 . hal-01298234

HAL Id: hal-01298234

https://hal.sorbonne-universite.fr/hal-01298234v1

Submitted on 5 Apr 2016

HAL is a multi-disciplinary open access archive for the deposit and dissemination of scientific research documents, whether they are published or not. The documents may come from teaching and research institutions in France or abroad, or from public or private research centers.

L'archive ouverte pluridisciplinaire **HAL**, est destinée au dépôt et à la diffusion de documents scientifiques de niveau recherche, publiés ou non, émanant des établissements d'enseignement et de recherche français ou étrangers, des laboratoires publics ou privés.

In vivo characterization of lamina cribrosa pore morphology in primary open-angle glaucoma

Caractérisation in vivo de la morphologie des pores de la lame criblée dans le glaucome primitif à angle ouvert

S. Zwillinger (MD) [12], M. Paques (MD; PHD) [123], B. Safran (MSc) [12], C. Baudouin (MD; PHD) [12345]

1. Quinze-Vingts National Ophthalmology Hospital, Paris France
2. Clinical Investigation Center INSERM 1423, Paris, France
3. Pierre and Marie Curie University Paris 6, Institut de la Vision, UMRS968, Paris France
4. Ambroise Paré Hospital, AP-HP, IFR Paris Ile de France Ouest
5. University of Versailles Saint-Quentin-en-Yvelines, Versailles, France

Corresponding author: Stephanie Zwillinger stephanie.zwillinger@gmail.com

Abstract

Purpose: To characterize the in vivo morphology of human lamina cribrosa pores in healthy and glaucoma eyes.

Patients and Methods: In this cross-sectional, observational study, a flood-illumination adaptive optics fundus (FIAO) camera was used to perform in vivo, high-resolution, noninvasive imaging of the optic disc and lamina cribrosa in 30 patients diagnosed with primary open-angle glaucoma (POAG), in 15 healthy controls and in 14 healthy subjects with at least one direct relative with POAG. Two masked graders measured each visible lamina cribrosa pores along the major and minor axes in order to categorize pores as oval (minor/major axis ratio <0.75) or round. We used these same measurements to calculate pore surface area as a best-fit oval.

Results: Lamina cribrosa pores were visible in 95.2% of the subjects. In 52% of controls, the pores were visualized under the neuroretinal rim. In POAG patients, 78% of visible pores had an oval aspect versus 19.4% in controls (p <0.01). Average pore surface area was significantly different (1,561 px^2 versus 724 px^2; p<0.01). In healthy subjects with at least one direct relative with POAG, 21% had pores with an aspect comparable to that of subjects in the glaucoma group.

Conclusion: On average, lamina cribrosa pores are elongated in POAG eyes and also in healthy eyes of POAG relatives. In vivo characterization of lamina cribrosa pore morphology by FIAO imaging may enhance our understanding of glaucoma, and offer new means for its early detection.

Keywords: Primary open-angle glaucoma, lamina cribrosa, adaptive optics

Résumé :

Objectif: Caractériser la morphologie in vivo des pores de la lame criblée de nerfs optiques de patients glaucomateux.

Patients et méthodes: Dans cette étude observationnelle transversale, une caméra à optique adaptative

a été utilisée pour effectuer in vivo une imagerie non invasive, de haute résolution du disque optique et de la lame criblée, chez 30 patients diagnostiqués avec un glaucome primitif à angle ouvert (GPAO), chez 15 contrôles sains et chez 14 sujets sains avec au moins un parent direct atteint de GPAO. Les données ont été recueillies en double aveugle, chaque pore visible de la lame criblée a été mesuré, le long des axes majeur et mineur afin de catégoriser les pores comme ovale ou rond. Nous avons utilisé ces mêmes mesures pour calculer la surface des pores.

Résultats: Chez 95,2% des sujets, les pores de la lame criblée étaient visibles. Chez 52% des contrôles, les pores ont été visualisés sous l'anneau neurorétinien. Chez les GPAO, 78% des pores visibles avaient un aspect ovale contre 19,4% chez les témoins ($p < 0,01$). La surface moyenne des pores était significativement différente (1,561 px^2 versus 724 px^2; $p<0.01$). Chez les sujets sains ayant au moins un parent direct atteint d'un GPAO, 21% avait des pores avec un aspect comparable à celui de sujets dans le groupe glaucome.

Conclusion: les pores de la lame criblée des patients GPAO ainsi que ceux des yeux des patients apparentés sont ovalaires. Ainsi la caractérisation in vivo de la morphologie des pores de la lame criblée en optique adaptative pourrait améliorer notre compréhension du glaucome, et offrir de nouveaux moyens pour sa détection précoce.

Mots clés : Glaucome primitif à angle ouvert, lame criblée, optique adaptative

Introduction

Primary open angle glaucoma (POAG) is a leading cause of blindness worldwide. It is a progressive optic neuropathy with structural changes in the optic disc, retinal nerve fiber layer (RNFL) and associated functional loss[1]. The mechanisms of glaucomatous alterations are still poorly understood, but the role played by the lamina cribrosa (LC) in the optic nerve head seems essential[2]. The LC is a three-dimensional porous structure composed of flexible collagenous tissue that supplies nutrition to the RNFBs via the connective tissue composed of astrocytes and a microvascular network located between the pores of the LC[3]. The LC is is a dynamic structure may be remodeled in response to the intraocular forces to which it is subjected[4,5].The assumed biomechanical response is cupping and sheering, which leads to changes in the LC surface in turn modifies the morphology of LC pores[6–9]. Deformation of LC pores is believed by some to be at the origin of the degradation of RNFBs in that it disrupts the axonal distribution as well as oxygenation and nutritional blood flow[10,11]. In glaucomatous patients the surface area and elongation of LC pores were measured in vivo using adaptive optics scanning laser ophthalmoscopy (AO-SLO)[12], enhanced depth imaging optical coherence tomography (EDI-OCT)[13,14], with clearly different morphological aspect between the healthy and glaucomatous LC, confirming previous studies results. 3D models of the LC have been developed to analyze its curvature and the subsequent changes in pore morphology[15,16]. The morphology of the LC pores can well be analyzed with an *en face* technology[17,18]. Studying the complex structure of the LC *in vivo* has therefore become central to glaucoma research [16,19,20].

Adaptive optics (AO) is a technology originally developed for astrophysics to improve the resolving power of ground-based telescopes. In ophthalmology, it has been used to measure and correct for the optical aberrations to provide near diffraction-limited imaging of the outer retina. It has already been successfully used in combination with OCT, SLO [21], and a fundus camera (flood illumination AO)[22]. AO-enhanced imaging technologies has been shown to be reproducible and reliable for measuring the LC

pores[23].

In the present study, we observed the LC using a flood-illumination AO (FIAO) camera. We sought to compare the morphology of LC pores between controls, POAG eyes and healthy subjects with at least one direct relative in the ascending line with POAG.

Patients and Methods

Cross-sectional, observational study. The subjects were either part of the consulting patient population at the Quinze-Vingts National Ophthalmic Center or members of the hospital's staff. Ethics Committee approval was received from Saint Antoine Hospital (Paris, France) as part of the iPhot project (ANR-09-TECS-009) and the study was conducted in strict accordance with the Declaration of Helsinki. Informed consent was obtained from all subjects after they received a complete explanation of this study's purposes.

Inclusion and exclusion criteria

For healthy subjects with no direct POAG relatives and healthy subjects with at least one direct relative in the ascending line with POAG, the following criteria were required: IOP <21 mmHg, best-corrected visual acuity (BCVA) of at least 20/20, FC imaging showing a clinically normal aspect of the OD, and no RNFL nor visual field (VF) deficit.

Inclusion criteria for the POAG group were IOP >22 mmHg at the time of first diagnosis, a glaucomatous appearance of the optic nerve disc (diffuse or localized rim thinning) and corresponding abnormalities observed during reliable visual field testing (considered reliable on the basis of $\leq$ 20% fixation loss, $\leq$ 15% false positives, and $\leq$ 33% false negatives).

Exclusion criteria for all participants were high myopia or hyperopia (±5D), ocular media opacities (including but not limited to cataract), nonglaucomatous optic neuropathy, any systemic diseases known

to affect the optic nerve structure including diabetes, pituitary tumor, uncontrolled hypertension, and family relationship.

Complete ophthalmic examination

Each study participant received a comprehensive ophthalmic examination including autorefraction, BCVA measurement (Landolt chart read at a distance of 5 m), slit-lamp examination, gonioscopy, Goldmann applanation tonometry, optic disc photography, OCT of the RNFL (Carl Zeiss Meditech, Oberkochen, Germany) and standard automated perimetry (SAP) through the Humphrey Visual Field Analyzer with the 24-2 Swedish Interactive Threshold Algorithm (HFA + 24-2 SITA; Carl Zeiss Meditec, Inc., Dublin, CA). All participants provided information regarding personal or familial medical history.

Imaging with adaptive optics

Each participant consented to OD imaging in the right eye with a FIAO camera (rtx1, Imagine Eyes, Orsay, France). The rtx1 camera acquires high-resolution images using an 850-nm flashed-flood source to illuminate the region of interest (ROI) to be imaged. The device acquires images equal to 4° × 4° (1.2 mm × 1.2 mm) on the retina with a maximum lateral resolution of 2 µm. Real-time video enables fine focusing, then a series (stack) of images is acquired during 4 s. Examinations were conducted in a dark room in order to facilitate imaging without pharmacological pupil dilation. An external target guiding the left eye was used to orientate the eye in order to observe the right optic disc.

We used Image J (National Eye Institute, Bethesda, MD, USA) to delineate and analyze the images using the pixel (px) as the unit of measurement. To determine the morphological characteristic of each pore, each grader manually drew the major and minor axes of each visible pore. The pore was considered circular if the ratio of minor over major axis was > 0.75 or oval if below. To calculate the surface area of LC pores, the measurements of all pores that passed the validation test in the preceding step were used to determine the size of the best-fit oval (BFO) (figure1).

The images were independently reviewed by two graders who were masked from all other subject information. Pore measurements were excluded if the graders did not reach consensus on both axes as defined by a set difference of ±15%.

Statistical analysis

To compare results, we used the Student's t test for quantitative variables and Fisher's exact test for nominal qualitative variables. We chose a critical cutoff value for the percentage of oval pores among the LC pores visible with AO-FC. The sensitivity and specificity versus cutoff graph was created using a sensitivity and specificity report. The Kappa coefficient was calculated to verify interobserver variations. All statistical analyses were conducted with commercially available software (StatView®[24]) and the type 1 error level was set at 0.05.

Results

Study population

59 subjects gave their consent to be investigated, comprising 15 healthy control subjects, with no direct relative in the ascending line with glaucomatous neuropathy (group 1), 30 POAG patients (group 2) and 14 healthy subjects with no familial relation with the other groups and who had at least one direct relative in the ascending line with glaucomatous neuropathy (group 3) (Table 1). All POAG patients were followed regularly prior to the study for at least 2 years and their IOP was measured under 21 mmHg with medical treatment at each follow-up visit.

Morphological study of the OD and LC in controls (group 1)

In all but two cases, LC imaging enabled more precise visualization of the LC when compared to images obtained with a FC. In these two cases, the LC was not visible, presumably because of RNFBs thickness. Most of the pores observed were circular in shape (Fig. 2). The minimum number of observable pores

was 3 and the maximum was 27. The minimum surface area was a BFO of 50 px², the largest was 2,994 px², and the average was 724 px² (Table 1). In this group, 19.4% of LC pores were to be oval and one subject had no oval-shaped pores at all. There was excellent agreement between graders as to whether an eye had an oval-shaped pore (kappa=0.8; 95% CI, 0.64–0.95). One optic disc was excluded because of the difficulties visualizing the pore limits, resulting in a significant difference in its measurements by the two graders.

Morphological study of the OD and LC in POAG subjects (group 2)

Thirty eyes were examined. There was no significant difference in age (p=0.062) and gender (p=0.75) between POAG subjects and healthy controls. Mean age was 54.3 years (±12.5 years) and 57% were female (Table 1). The LC was visible by FIAO imaging in all eyes. Most of the pores were enlarged, elongated and fused (Fig. 3). We also noted an apparent torsion of pores close to the scleral rim. In one subject with advanced POAG, the pores had almost completely disappeared. The minimum number of measurable pores was 9 and the maximum was 41. The minimum surface area was a BFO of 36 px², the maximum was 13,558 px², and the average was 1,561 px². In this group, 78% of LC pores were oval (kappa=0.8; 95% CI, 0.64–0.95). The average surface area of LC pores was notably greater in group 2 than in group 1 (Table 1) in POAG subjects versus healthy controls (1,561 px² and 724 px², respectively, P<0.0028). In POAG subjects, 78% of pores were oval versus 19.4% in healthy controls (p<1.5 10^{-7}). The cutoff value of 60% maximized sensitivity (100%) and specificity (79%) (CI=95%).

Morphological study of the LC in group 3

Fourteen eyes were examined. Their age was significantly lower than in the other two groups. This significant difference prevented us from conducting a valid statistical analysis between these three groups. Of the 14 subjects in this group, three had LC pores with an aspect comparable to that of subjects in the POAG group, as more than 60% of pores were oval and the average surface area of those

pores was 1,196 px² (Fig.4). Two had LC with no visible pores. Nine subjects in this group displayed an aspect of the LC comparable with that in healthy controls. The average surface area of those pores was 637 px² and less than 60% of pores were oval, although all nine had some oval LC pores (kappa=0.8; 95% CI, 0.64–0.95).

Discussion

Interest in LC pore study is gaining momentum, because it is assumed to be the primary location of retinal nerve fiber glaucomatous damage. FIAO imaging is a promising technique for analyzing LC pores. Previous in vivo studies[2,21] and more recently studies using three dimensional characterization of the LC, have shown that pores in POAG eyes subjects tend to be larger and elongated[25]. Analyses of LC pore dynamics in POAG have suggested that they rotate near the scleral opening, where compression forces are strongest, thus leading to the fusion of peripheral pores[26].

It has not yet been confirmed if the changes in pore morphology in POAG eyes is a cause or a consequence of the disease. However, recent studies have advanced the idea that some LCs may have structural weakness[27–29]. In these cases, axonal degradation may be caused by the loss of their support inside the LC, for instance insufficient nutrition from the microvascular network and/or the loss of contact with astrocytes[30].

All of the aforementioned studies point to the fact that LC pores in glaucomatous subjects becomes larger and elongated. We obtained similar results in this study. Concerning the examination of subjects with at least one direct relative in the ascending line with POAG, it could corroborate an inherited weakness of the LC[31–33].

This technique has several limitations. The FIAO imaging field is limited and therefore requires acquisition of multiple images in order to visualize more than the pores of the LC. Pores may have been

missed because of poor visibility of the LC, especially in healthy eyes, 13% of which were excluded. The LC is a three dimensional structure. Posterior cupping may have changed the angle of incidence between the laminar surface and the imaging axis, hence inducing errors in measurements in pore dimensions[16,18].

In order to understand the morphological modifications to the LC that are specific to glaucomatous neuropathy, it is essential to clearly characterize the difference between healthy and pathological LCs and define a morphological characteristic that would better correspond to a glaucomatous LC pore pattern. The FIAO cmarea used in this study enabled us to clearly measure a difference between two types of pores – round and oval – that is coherent with other in vivo observations. The proportion of LC pores considered to be oval using our method allowed us to determine a cutoff value based on the percentage of oval pores among the visible pores. The examination of subjects with at least one direct relative in the ascending line with familial history of POAG (group 3) allowed us to test our hypothesis and to propose responses regarding the origins of the LC pore shape. We found that three out of these subjects had more than 60% oval-shaped pores. The youngest of those subjects was 9 years of age. In the nine remaining subjects, less than 60% of LC pores were considered oval. In the first three cases, these early alterations of the LC pores were detected before the suspected changes that would affect the RNFLs. A closer follow-up routine with repeated IOP measurements will be proposed to these subjects to detect whether any signs of glaucomatous neuropathy develop further.

Thanks to this technique and our findings in descendants of POAG patients, the respective roles of IOP and LC morphological changes, thus in POAG pathogenesis, could be clarified by a further prospective study. The percentage of oval LC pores may thus be a warning signal requiring closer and more regular medical examination. However, only a long-term prospective study with a larger population would be able to confirm whether this morphological aspect is truly an early sign of impending glaucomatous neuropathy, a risk factor – whether or not it results in further IOP elevation during the subject's lifetime

– or only coincidence. This morphological pattern could translate into a genetic phenotype to identify subjects who have inherited one or several risk factors for POAG.

References

1. Burgoyne CF, Morrison JC. The anatomy and pathophysiology of the optic nerve head in glaucoma. *J Glaucoma*. 2001;10(5 Suppl 1):S16-S18.

2. Miller KM, Quigley HA. The clinical appearance of the lamina cribrosa as a function of the extent of glaucomatous optic nerve damage. *Ophthalmology*. 1988;95(1):135-138.

3. Downs JC, Roberts MD, Burgoyne CF. Mechanical environment of the optic nerve head in glaucoma. *Optom Vis Sci Off Publ Am Acad Optom*. 2008;85(6):425-435.

4. Roberts MD, Sigal IA, Liang Y, et al. Changes in the biomechanical response of the optic nerve head in early experimental glaucoma. *Invest Ophthalmol Vis Sci*. 2010;51(11):5675-5684.

5. Strouthidis NG, Grimm J, Williams GA, et al. A comparison of optic nerve head morphology viewed by spectral domain optical coherence tomography and by serial histology. *Invest Ophthalmol Vis Sci*. 2010;51(3):1464-1474.

6. Burgoyne CF, Downs JC, Bellezza AJ, et al. The optic nerve head as a biomechanical structure: a new paradigm for understanding the role of IOP-related stress and strain in the pathophysiology of glaucomatous optic nerve head damage. *Prog Retin Eye Res*. 2005;24(1):39-73.

7. Roberts MD, Liang Y, Sigal IA, et al. Correlation between local stress and strain and lamina cribrosa connective tissue volume fraction in normal monkey eyes. *Invest Ophthalmol Vis Sci*. 2010;51(1):295-307.

8. Roberts MD, Grau V, Grimm J, et al. Remodeling of the connective tissue microarchitecture of the lamina cribrosa in early experimental glaucoma. *Invest Ophthalmol Vis Sci*. 2009;50(2):681-690.

9. Burgoyne CF, Downs JC. Premise and prediction-how optic nerve head biomechanics underlies the susceptibility and clinical behavior of the aged optic nerve head. *J Glaucoma*. 2008;17(4):318-328.

10. Crawford Downs J, Roberts MD, et al. Glaucomatous cupping of the lamina cribrosa: a review of the evidence for active progressive remodeling as a mechanism. *Exp Eye Res*. 2011;93(2):133-140.

11. Dai C, Khaw PT, Yin ZQ, Li D, et al. Structural basis of glaucoma: the fortified astrocytes of the optic nerve head are the target of raised intraocular pressure. *Glia*. 2012;60(1):13-28.

12. Vilupuru AS, Rangaswamy NV, Frishman LJ, et al. Adaptive optics scanning laser ophthalmoscopy for in vivo imaging of lamina cribrosa. *J Opt Soc Am A Opt Image Sci Vis*. 2007;24(5):1417-1425.

13. Park H-YL, Jeon SH, Park CK. Enhanced depth imaging detects lamina cribrosa thickness differences in normal tension glaucoma and primary open-angle glaucoma. *Ophthalmology*. 2012;119(1):10-20.

14. Tatham AJ, Miki A, Weinreb RN, et al. Defects of the lamina cribrosa in eyes with localized retinal nerve fiber layer loss. *Ophthalmology*. 2014;121(1):110-118.

15. Burgoyne CF, Downs JC, Bellezza AJ, et al. Three-dimensional reconstruction of normal and early glaucoma monkey optic nerve head connective tissues. *Invest Ophthalmol Vis Sci*. 2004;45(12):4388-4399.

16. Sredar N, Ivers KM, Queener HM, et al. 3D modeling to characterize lamina cribrosa surface and pore geometries using in vivo images from normal and glaucomatous eyes. *Biomed Opt Express*. 2013;4(7):1153-1165.

17. Kimura Y, Akagi T, Hangai M, et al. Lamina cribrosa defects and optic disc morphology in primary open angle glaucoma with high myopia. *PloS One*. 2014;9(12):e115313.

18. Shoji T, Kuroda H, Suzuki M, et al. Correlation between Lamina Cribrosa Tilt Angles, Myopia and Glaucoma Using OCT with a Wide Bandwidth Femtosecond Mode-Locked Laser. *PloS One*. 2014;9(12):e116305.

19. Kiumehr S, Park SC, Syril D, et al. In vivo evaluation of focal lamina cribrosa defects in glaucoma. *Arch*

Ophthalmol. 2012;130(5):552-559.

20. Nadler Z, Wang B, Wollstein G, et al. Repeatability of in vivo 3D lamina cribrosa microarchitecture using adaptive optics spectral domain optical coherence tomography. *Biomed Opt Express*. 2014;5(4):1114-1123.

21. Akagi T, Hangai M, Takayama K, et al. In vivo imaging of lamina cribrosa pores by adaptive optics scanning laser ophthalmoscopy. *Invest Ophthalmol Vis Sci*. 2012;53(7):4111-4119.

22. Sarda V, Nakashima K, Wolff B, et al. Topography of patchy retinal whitening during acute perfused retinal vein occlusion by optical coherence tomography and adaptive optics fundus imaging. *Eur J Ophthalmol*. 2011;21(5):653-656.

23. Ivers KM, Li C, Patel N, et al. Reproducibility of measuring lamina cribrosa pore geometry in human and nonhuman primates with in vivo adaptive optics imaging. *Invest Ophthalmol Vis Sci*. 2011;52(8):5473-5480.

24. *Statview@*. Version 6. Cary, North Carolina, US: SAS Institute Inc.

25. Nadler Z, Wang B, Schuman JS, et al. In vivo three-dimensional characterization of the healthy human lamina cribrosa with adaptive optics spectral-domain optical coherence tomography. *Invest Ophthalmol Vis Sci*. 2014;55(10):6459-6466.

26. Bellezza AJ, Rintalan CJ, Thompson HW, et al. Deformation of the lamina cribrosa and anterior scleral canal wall in early experimental glaucoma. *Invest Ophthalmol Vis Sci*. 2003;44(2):623-637.

27. Ma F, Dai J, Sun X. Progress in understanding the association between high myopia and primary open-angle glaucoma. *Clin Experiment Ophthalmol*. 2014;42(2):190-197.

28. Jung KI, Jung Y, Park KT, et al. Factors affecting plastic lamina cribrosa displacement in glaucoma patients. *Invest Ophthalmol Vis Sci*. 2014;55(12):7709-7715.

29. Kang MH, Law-Davis S, Balaratnasingam C, et al. Sectoral variations in the distribution of axonal cytoskeleton proteins in the human optic nerve head. *Exp Eye Res*. 2014;128:141-150.

30. Balaratnasingam C, Kang MH, Yu P, et al. Comparative quantitative study of astrocytes and capillary distribution in optic nerve laminar regions. *Exp Eye Res*. 2014;121:11-22.

31. Liu T, Xie L, Ye J, et al. Family-based analysis identified CD2 as a susceptibility gene for primary open angle glaucoma in Chinese Han population. *J Cell Mol Med*. 2014;18(4):600-609.

32. Huang W, Fan Q, Wang W, et al. Collagen: a potential factor involved in the pathogenesis of glaucoma. *Med Sci Monit Basic Res*. 2013;19:237-240.

33. Dong L-Y, Yin M, Kang X-L. Bibliometric network analysis of glaucoma. *Genet Mol Res GMR*. 2014;13(2):3577-3585.

Figure 1 : Measurement procedure of lamina cribrosa (LC) pores. Left, the optic disc as seen with FIAO imaging; right, morphometric analysis.

Figure 2: FIAO images of the LC in two healthy control subjects.

Figure 3: Example of FIAO imaging of the LC of two POAG subjects.

Figure 4: Example of FIAO imaging of the LC of two healthy subjects with at least one direct relative in the ascending line with POAG.

Michel Paques is a consultant for Imagine Eyes.

	Group 1	Group 2	Group 3	Test	*p* between groups 1 and 2
Eyes	15	30	14		
Age (years ± SD)	46.8 ± 19.5	54.3+/- 12.5	21.4 +/-8.2	Student *t*-test	0.062
Female gender Number (%)	10 (67%)	17(57%)	12(83%)	Fischer exact test	0.75
Mean number of pores ±SD	11.9 ± 7.6	24.9 ± 8.7	23.7 ± 10	Student *t*-test	$7{,}7\ 10^{-5}$
Mean BFO (px^2) ± SD	724 ± 519	1,561 ± 1,176	777 ± 527	Student *t*-test	0.0028
BFO (px^2) (range)	(50–2,994)	(36–13,558)	(53–6,660)		
Percent of oval pores ± SD	19.4 ± 18.8	78 ± 12	45.0±26.1	Student *t*-test	$1.5\ 10^{-7}$

Table 1: Demographic and clinical characteristics of the three groups (BFO: best fitted oval in px^2)

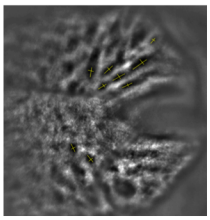

- **Aspect ratio** $= \frac{MAX(\emptyset X;\ \emptyset Y)}{MIN(\emptyset X;\ \emptyset Y)}$

$\emptyset X = (X1 + X2 + X3)$

$\emptyset Y = (Y1 + Y2 + Y3)$

Circular (C): Aspect ratio ≥ 0.75:1.00 (<75%)

Ovular (O): aspect ratio ≤ 0.75:1.00 (>75%)

Average surface of LC pore

BFO $= \frac{\emptyset X}{2} \times \frac{\emptyset Y}{2} \times \pi$

Figure 1

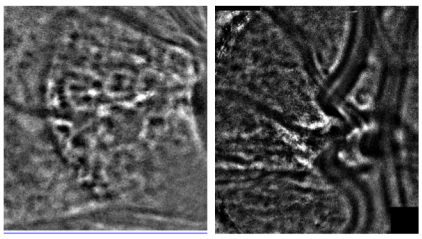

Figure 2

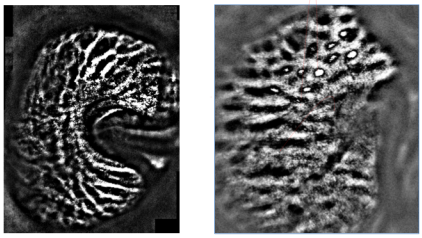

Figure 3

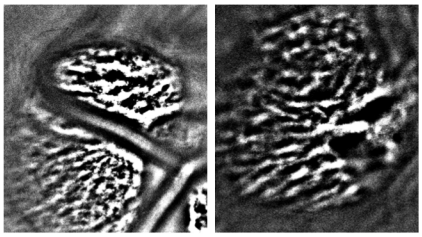

Figure 4